Intermolecular Packing in Stereoregular Polypropylene Liquids: Comparison between Theory and X-ray Scattering Experiments†

John G. Curro,* Jeffrey D. Weinhold, and John J. Rajasekaran‡

Sandia National Laboratories, Albuquerque, New Mexico 87185-0333

A. Habenschuss and J. D. Londono

Oak Ridge National Laboratory, Oak Ridge, Tennessee 37831

J. Dana Honeycutt

Molecular Simulations Inc., 9685 Scranton Road, San Diego, California 92121-3752

Received April 11, 1997⊗

ABSTRACT: Atomistically realistic polymer reference interaction site model (PRISM) calculations on isotactic and syndiotactic polypropylene liquids were compared with wide-angle X-ray scattering measurements at 180 and 183 °C. The intramolecular structure factors, required as input to PRISM theory, were obtained from single-chain, Monte Carlo simulations using three models with progressively more realism: a rotational isomeric state model, a united atom model, and an explicit atom model. Excellent agreement between PRISM theory, employing the united and explicit atom models, was found with the experimentally determined structure factor in the wavevector range $0.3\ \text{Å}^{-1} \le k \le 16\ \text{Å}^{-1}$. Good agreement was also seen between theory and experiment for the average intermolecular radial distribution function in *r*-space estimated from the Fourier transform of the scattering data. The rotational isomeric state model predicted a structure factor qualitatively inconsistent with the scattering experiments. This suggests that continuously varying rotations are important in the packing of vinyl polymers. The six individual site−site intermolecular pair correlation functions calculated from PRISM theory show universal behavior on long length scales in the correlation hole regime but reveal significant system specific differences in structure on short length scales near contact. At short distances, the pendant methyl groups on the polypropylene backbone tend to shield the backbone groups from approaching each other closely in the melt. Subtle differences were seen in the pair correlation functions between isotactic and syndiotactic polypropylene on local length scales.

I. Introduction

Polyolefin blends show a rich dependence of miscibility on the molecular architecture of the individual components.[1−4] Recent theoretical calculations[5−9] using the polymer reference interaction site model (PRISM theory) suggest that subtle intermolecular packing effects can have a profound effect on the miscibility characteristics of polymer blends in the melt state. It would seem, therefore, that in order to understand miscibility in blends, one must first have a knowledge of the packing in the one-component, homopolymer melt. It has been demonstrated previously[10,11] that PRISM theory gives an excellent description of the structure of polyethylene melts determined by wide-angle X-ray scattering. The purpose of the present investigation is to test the ability of PRISM theory to describe the packing in more complex polyolefin melts. In this paper we calculate the structure of stereoregular polypropylene melts using PRISM theory with an atomistically realistic model and compare with the structure factor obtained from wide angle X-ray scattering experiments.

Isotactic polypropylene (i-PP) melts have been investigated previously by small angle neutron scattering[12−13] (SANS). On the basis of this early work, the characteristic ratio C_∞ ($= \langle r^2 \rangle / nl^2$, where *r* is the end-to-end distance and *n* is the number of backbone bonds of length *l*) was found to be approximately 6.2 with the radius of gyration being essentially independent of temperature. Recent work by Weimann and co-workers[14] suggests that C_∞ might be somewhat smaller in a blend of i-PP and Poly(ethylene/ethylethylene) random copolymer. Recent SANS measurements on atactic polypropylene (a-PP) by Zirkel and co-workers[15] lead to a characteristic ratio in the range 5.4−6.0 with a negative temperature coefficient of the radius of gyration $\mathrm{d}(\ln R_g)/\mathrm{d}T = -0.12 \times 10^{-3}$ K. Although we are not aware of any SANS measurements on syndiotactic polypropylene (s-PP), intrinsic viscosity measurements by Inakagi[16] and co-workers in 1966 suggest the characteristic ratio to be about 6.8. It should be kept in mind, however, that a high degree of stereoregularity may not have been achievable in s-PP samples made at that time.[15] Preliminary wide-angle X-ray scattering measurements on a range of polyolefins, including isotactic and syndiotactic polypropylene, have been reported by Londono and co-workers.[17] Differences can be seen among the polyolefins in the low-angle region despite the similarities in polymer structure. This reflects intermolecular packing differences due to the architecture of the polymer chains.

PRISM theory[18] has the ability to account for intermolecular packing on both long and short length scales. All information regarding the polymer architecture enters the theory through the single chain structure factors, usually obtained from a separate single chain calculation or simulation. For long-range packing on a radius of gyration length scale, one can employ computationally convenient, coarse grained models to provide the single chain structure. On smaller length scales comparable to a few monomer diameters, however, it is

† Work at Sandia National Laboratories supported by the U. S. Department of Energy under Contract No. DE-AC04-94AL85000. Work at Oak Ridge National Laboratory supported by the U. S. Department of Energy under Contract No. DE-AC05-96OR22464.

‡ Present address: Intel Corporation, Albuquerque, NM.

⊗ Abstract published in *Advance ACS Abstracts,* September 1, 1997.

S0024-9297(97)00500-7 CCC: $14.00

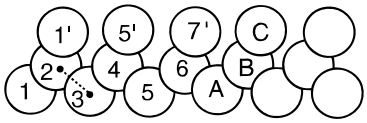

Figure 1. Schematic representation of the united atom model for polypropylene. Sites A, B, and C refer to the CH_2, CH, and CH_3 groups respectively. Either the isotactic or syndiotactic forms of the molecule are maintained in the calculations. 1−4 types of interactions are included by the rotational potential in eq 6 for rotations ϕ about covalent bonds such as between sites 2 and 3. Interactions between 1−5 and 1−6 types of sites are included using the Lennard−Jones potential in eq 7 of the text. Longer range interactions along the chain backbone, eg. 1−7, 1−8, etc., are set to zero.

necessary to include the chemical details of the monomer architecture in computing the required single chain structure functions. Honnell and co-workers[10,11] found that a rotational isomeric state model, used as input to PRISM theory, could accurately predict the structure factor of polyethylene melts. In contrast, the asymmetric nature of the monomer structure cannot easily be described by a simple rotational isomeric state model in polypropylene. In fact, there are at least eight different rotational isomeric state models[15] for i-PP that give vastly different characteristic ratios ranging from 4.2 to 9.4.

In the present study we will investigate three distinct methods for obtaining the required intramolecular structure input to PRISM theory: (1) the rotational isomeric state model for i-PP of Suter and Flory,[19] (2) a united atom chain model for i-PP and s-PP with continuous rotational potentials, and (3) an explicit atom model for i-PP which specifically includes all the carbon and hydrogen atoms in the chain. In each of these methods we will make use of the well-known Flory ideality theorem stating that long-range excluded volume interactions are screened in polymer melts. The structure functions for these models will be obtained from single chain, Monte Carlo simulations and used as input to PRISM theory. Direct comparisons will be made with the total structure factor from X-ray scattering measurements, and with an average radial distribution function derived from the X-ray scattering data.

II. PRISM Theory

Polymer RISM theory has been discussed[18,20−22] extensively in previous publications. Here we will briefly summarize the formalism as applied to vinyl polymer melts. PRISM theory is an extension to polymers of the reference interaction site model or RISM theory of Chandler and Andersen.[23,24] Recently Curro[25] treated freely jointed vinyl polymer liquids using PRISM theory; the extension to atomistically realistic chain models is straightforward. We represent a polypropylene macromolecule using a three-site model depicted schematically in Figure 1. Each monomer repeat unit consists of three independent, overlapping sites, A, B, and C, corresponding to CH_2, CH, and CH_3 moieties, respectively. For a system of N_c chains, each containing N monomers, the intermolecular packing can be characterized in terms of radial distribution functions defined as

$$\tilde{\rho}^2 g_{\alpha\gamma}(r) = \left\langle \sum_{i\neq j=1}^{N_c} \delta(\vec{r}_i^{\,\alpha})\, \delta(\vec{r} - \vec{r}_j^{\,\gamma}) \right\rangle \tag{1}$$

where $\tilde{\rho} = N_c/V$ is the chain density and $\vec{r}_i^{\,\alpha}$ is the position vector of site α on chain i. If we neglect end effects,[22] each monomer along the chain backbone is equivalent and hence there are only six distinct radial distribution functions $g_{mm'}(r)$

$$g_{mm'}(r) = g_{\alpha\gamma}(r) \qquad \alpha \in m,\ \gamma \in m' \tag{2}$$

where the indices m and m′ correspond to the types of sites A, B, or C.

Following Chandler and Andersen,[23,24] we can define[25] a set of direct correlation functions $C_{mm'}(r)$ from a generalized Ornstein−Zernike equation which we write for convenience in Fourier transform space as

$$\hat{\mathbf{h}}(k) = \hat{\mathbf{\Omega}}(k)\mathbf{C}(k)[\hat{\mathbf{\Omega}}(k) + \rho\hat{\mathbf{h}}(k)] \tag{3}$$

where the caret denotes Fourier transformation with wavevector k. In eq 3, $\rho = N\tilde{\rho}$ is the monomer density, and $h_{mm'}(r)$ and $C_{mm'}(r)$ are 3 × 3 symmetric matrices involving correlations between pairs of sites of type A, B, or C. All information regarding the intramolecular chain architecture enters the theory through the intramolecular structure functions $\hat{\Omega}_{mm'}(k)$ defined according to

$$\hat{\Omega}_{mm'}(k) = \frac{1}{N}\sum_{i\in m}\sum_{j\in m}\hat{\omega}_{ij}(k) = \frac{1}{N}\sum_{i\in m}\sum_{j\in m}\left\langle \frac{\sin kr_{ij}}{kr_{ij}} \right\rangle \tag{4}$$

where $\omega_{ij}(r)$ is the normalized probability density between a pair of sites i and j along a single polypropylene chain.

In order to solve eq 3 for the six radial distribution functions $g_{AA}(r)$, $g_{BB}(r)$, $g_{CC}(r)$, $g_{AB}(r)$, $g_{AC}(r)$, and $g_{BC}(r)$, we employ the approximate Percus−Yevick-like closure[18]

$$C_{mm'}(r) = \{1 - \exp[\beta v_{mm'}(r)]\}g_{mm'}(r) \tag{5a}$$

where $v_{mm'}(r)$, is the potential between sites of type m and m′ and $\beta = 1/k_BT$. For hard core potentials, eq 5a reduces to the particularly simple form

$$g_{mm'}(r) = 0 \quad \text{for } r < d_{mm'} \qquad C_{mm'}(r) = 0 \quad \text{for } r > d_{mm'} \tag{5b}$$

with hard core diameters $d_{mm'}$. Equations 3−5 lead to a set of six coupled integral equations which can be solved by standard Picard iteration techniques[25] for the radial distribution functions characterizing the intermolecular packing in the liquid.

In general, one would expect the intramolecular structure functions $\hat{\Omega}_{mm'}(k)$ to be coupled to the intermolecular structure characterized by $g_{mm'}(r)$ in the melt. This coupling would necessitate that the intra- and intermolecular structure be solved in a self-consistent manner. Although this self-consistency calculation is possible,[18] one can to good approximation make use of Flory's idea[26] that long range excluded volume interactions are screened in the melt. That a polymer melt acts like a θ solvent for itself has been demonstrated through SANS experiments[27] and computer simulations.[28] With this ideality approximation, the functions $\hat{\Omega}_{mm'}(k)$ can be evaluated in a separate, single-chain calculation or simulation, where the long-range repulsive interactions along the chain are set to zero. The intramolecular structure functions obtained in this manner are then used as input to eq 3 which, together

Table 1. Geometrical Parameters Used in the Single-Chain Simulations of PP

tacticity	model	L[a]	ABA[b]	BAB[b]	ABC[b]	CBA[b]
i-PP	RIS	1.54	112.0	112.0	106.8	106.8
i-PP	united atom	1.54	111.5	118.2	112.4	108.8
i-PP	explicit atom	1.54	111.5	118.2	112.4	108.8
s-PP	united atom	1.54	111.8	114.6	111.0	111.0

[a] Bond lengths in Å. [b] Bond angles between sites in deg.

with eq 5, yields the radial distribution functions. Thus, PRISM theory can be seen to provide a link between intramolecular structure and intermolecular packing.

III. Intramolecular Structure

One of the objectives of the present study is to determine how best to compute the intramolecular structure functions $\hat{\Omega}_{mm'}(k)$. A balance between atomistic rigor and computational convenience is needed. Here we attempt to determine the level of detail in the monomeric structure that is necessary in order to accurately describe the intermolecular packing through PRISM theory. Toward this end we studied three polymer models for i-PP that include varying extents of chemical detail in the monomeric structure. The adequacy of each model can be assessed by (i) comparing the intramolecular structure and packing calculated for each model and (ii) by comparison of the predictions of each model with X-ray scattering experiments.

Rotational Isomeric State Model. Honnell and coworkers[10,11] achieved considerable success in modeling polyethylene melts with a rotational isomeric state model[29] involving one trans and two gauche rotational states. The $\hat{\Omega}_{mm'}(k)$ functions can be determined[30] from a Monte Carlo simulation on a single chain molecule, or by an approximate "patching technique". The usefulness of the rotational isomeric state approach is diminished for vinyl chain molecules because more isomeric states are required, and the angular location of the states often is not physically obvious as in the case of polyethylene. There have been numerous rotational isomeric state models[15] employed for i-PP, giving drastically different characteristic ratios. For demonstration purposes here we chose to employ the model of Suter and Flory[19] which has five discrete dihedral angles at 15, 50, 70, 105, and −115°. The fixed backbone bond lengths and angles are given in Table 1. The six independent $\hat{\Omega}_{mm'}(k)$ functions were evaluated from a Monte Carlo simulation on a single i-PP chain of $N = 200$ monomers. In keeping with the Flory ideality hypothesis discussed above, no long range excluded volume was included in the simulation beyond the "pentane effect".

The original energetic parameters used by Suter and Flory lead to a characteristic ratio considerably less than 6.2 at the experimental temperature of 473 K. To correct for this discrepancy we reproduced the experimental characteristic ratio by adjusting the temperature in the simulation to 286 K. Such a procedure is equivalent to rescaling the energy parameters (by 1.65) in the Suter and Flory model. The results of this computation are depicted in Figure 2 for $\hat{\Omega}_{AA}(k)$ and $\hat{\Omega}_{CC}(k)$. The rotational isomeric state model employed here is the same one used earlier by Rajasekaran and co-workers[8] in calculating the miscibility characteristics of polyethylene/i-PP blends via PRISM theory. It should be emphasized that this rescaling of energies was only applied to the rotational isomeric state model in order to make comparisons with experiment more meaningful. Such a procedure was not applied to the united or explicit atom models described below.

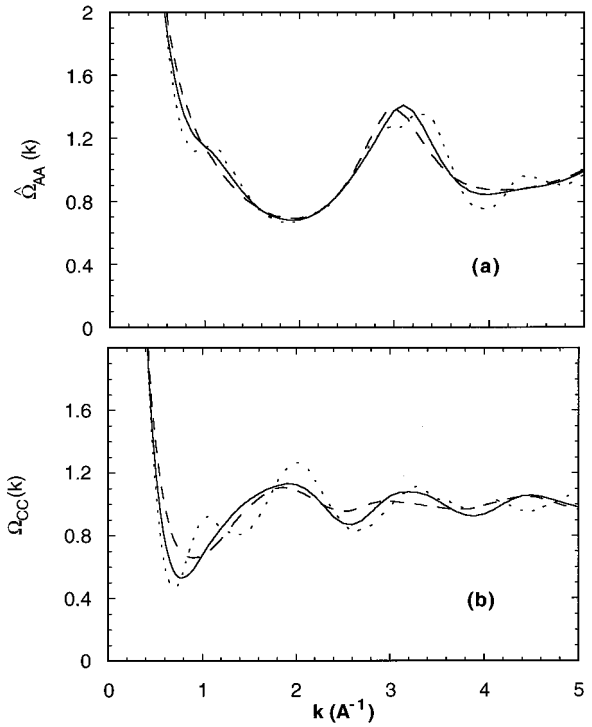

Figure 2. Intramolecular structure functions for i-PP as a function of wavevector **k**: dotted curve, rotational isomeric state model; solid curve, united atom model; dashed curve, explicit atom model. Key: (a) AA correlations; (b) CC correlations.

United Atom Model. With modern computers the task of modeling a single polymer chain with continuous rotational potentials is not significantly more difficult than for discrete rotations. For this reason we included more realism in our intramolecular simulation by allowing the dihedral angles in the polypropylene chain to undergo continuous rotations. In these simulations we used a united atom representation in which the hydrogen atoms are absorbed into 3 sites A, B, and C corresponding to CH_2, CH, and CH_3 groups respectively as in Figure 1. Both the isotactic and syndiotactic forms of polypropylene were studied. The bond angles and bond lengths were held fixed in the Monte Carlo simulations with values indicated in Table 1.

1−4 type interactions (between sites separated by 3 bonds, see Figure 1) were included through the rotational potential due to Jorgensen and co-workers[31] for isopentane, the small molecule analog of polypropylene.

$$V(\phi) = V_o + \frac{V_1}{2}[1 + \cos(\phi \pm 120)] + \frac{V_2}{2}[1 + \cos 2(\phi \pm 120)]\ V_3 2[1 + \cos 3(\phi \pm 120)] \quad (6)$$

In eq 6, for i-PP the + option is used for backbone rotational angles ϕ with the CH_2 group on the right, and the − option for angles ϕ with the CH_2 on the left; for s-PP the + option is used for all backbone rotations. The Jorgensen energies of 2713, 1526, 533, and −3453 cal/mol were used for V_o, V_1, V_2, and V_3 respectively.[31]

1−5 and 1−6 types of interactions between sites (separated by four or five bonds, see Figure 1) were accounted for by Lennard−Jones potentials.

$$v_{mm'}(r) = 4\epsilon_{mm'}\left[\left(\frac{\sigma_{mm'}}{r}\right)^{1/2} - \left(\frac{\sigma_{mm'}}{r}\right)^{6}\right] \quad (7)$$

Table 2. United Atom, Lennard−Jones Parameters between 1−5 and 1−6 Types of Sites

tacticity	param	A (CH_2)	B (CH)	C (CH_3)
i-PP	σ (Å)	4.1393	4.0810	3.5762
	ϵ/k_B (K)	59	40	80
s-PP	σ (Å)	3.5536	3.5035	3.0701
	ϵ/k_B (K)	59	40	80

The ϵ_{mm} parameters of Jorgensen shown in Table 2 were employed. Bertholet scaling was assumed for the cross terms, $\epsilon_{mm'} = (\epsilon_{mm}\epsilon_{m'm'})^{1/2}$. The σ parameters were then adjusted in order to reproduce the experimental value of the characteristic ratio of 6.2 for i-PP and 6.8 for s-PP in the simulations. The parameters used in the simulations are indicated in Table 2. Note that σ_{CC} associated with interactions between pendant methyl groups is seen to be smaller than expected (3.5762Å) based on the Jorgensen potentials. This probably reflects the fact that methyl groups on adjacent monomers along the chain backbone can interlock to some extent.[33] σ_{AA} and σ_{BB} were found to be 1.06 (0.91) times the corresponding Jorgensen values for i-PP (s-PP). The cross terms were approximated by $\sigma_{mm'} = (\sigma_{mm} + \sigma_{m'm'})/2$.

It is well-known[26−28] that long range excluded volume interactions are screened in a polymer melt; thus it would be incorrect to include repulsive interactions between all pairs of sites along the chain backbone without a corresponding medium-induced potential to mitigate the excluded volume interactions. In the present investigation we will mimic a chain in the melt by purposely setting repulsive interactions to zero beyond some arbitrary cutoff. Such a procedure[35] is a generalization to what is done in the well-known rotational isomeric state approximation. Here we somewhat arbitrarily use a cutoff distance of 6 bonds and simply set repulsive 1−7 and higher types of interactions to zero, thereby recovering the ideal chain scaling of R_g with N characteristic of the melt. A more realistic procedure, in which a self-consistent, medium-induced potential is employed, is possible[18] but beyond the scope of the present investigation.

United atom, Monte Carlo simulations were performed for $N = 200$ monomers with the chain parameters shown in Table 1. The parameters for i-PP were chosen to correspond as closely as possible with the corresponding explicit atom model discussed in the next section. Figure 2 depicts the i-PP united atom simulation results for $\hat{\Omega}_{AA}(k)$ and $\Omega_{CC}(k)$ in k-space. Figure 3 shows the corresponding functions $\Omega_{AA}(r)$ and $\Omega_{CC}(r)$ in real space.

Explicit Atom Model. The most atomistically realistic model we studied is denoted as the explicit atom model. This model is similar to the united atom model except that it explicitly includes the hydrogen atoms. The bond lengths and angles were first determined by minimizing a chain in a 3/1 helical conformation for i-PP and an all-trans conformation for s-PP using a variant of the molecular simulations consistent force field[34] (CFF) known as PCFF (for "polymer consistent force field"). This is an all-atom force field that contains internal (bond, angle, torsion, cross-terms), van der Waals (6−9 Lennard−Jones) and coulombic terms. The force field was derived by first determining internal terms and partial atomic charges from ab initio quantum calculations. Then scaling factors were applied to best fit the experimental spectra. The van der Waals terms were determined from small molecule crystal data. See ref 34 for details.

After minimization with PCFF, the bond lengths and angles were held fixed at the values indicated in Table 1 during the Monte Carlo simulation. The asymmetry in the values of the ABC and CBA angles in Table 1 arises from the asymmetry of the 3/1 helix. Such a helix can be right-handed or left-handed. Reversing the handedness of the helix and re-minimizing causes the ABC and CBA angles to switch. The simulation method used to determine the single chain structure functions was the "rotational isomeric state" Metropolis Monte Carlo (RMMC) method.[35] This is a torsion-space technique that adopts the short-range interaction assumption of rotational isomeric state theory, but allows the backbone torsion angles to vary continuously, rather than only discretely. During the simulation, the pendant methyl groups did not rotate but were held fixed at an optimum angle also determined from the energy minimization.

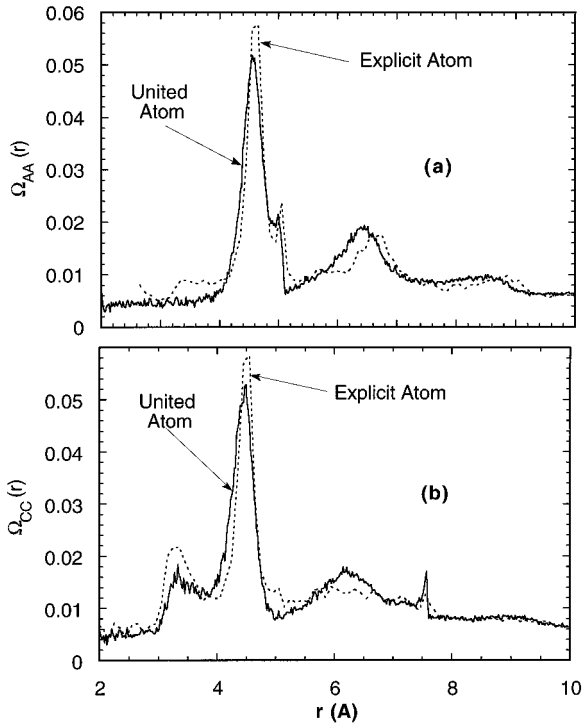

Figure 3. Intramolecular structure functions for i-PP as a function of r: solid curve, united atom model; dashed curve, explicit atom model. For clarity, intramolecular correlations between sites separated by 1 and 2 bonds were not included. Key: (a) AA correlations; (b) CC correlations.

The PCFF force field was used for torsion terms and nonbonded interactions for atoms separated by four or five bonds. As in the united atom model, interactions between atoms separated by six or more bonds were set to zero in order to mimic a chain in a melt. To mediate the electrostatic interactions, an effective dielectric constant of 1.5 was found to give a characteristic ratio in agreement with the experimental values. A consequence of not including 1−7 and higher interactions is that hydrogen atoms on the methyl groups of adjacent monomers do not interact. This mimics the tendency of methyl groups to interlock[33] as in the united atom case above, in that exclusion of the H−H interactions reduces the effective CH_3-CH_3 interaction radius. Simulations were performed on i-PP chains consisting of $N = 200$ monomers.

The i-PP results from the 3 models are compared for $\hat{\Omega}_{AA}(k)$ in Figure 2a and $\hat{\Omega}_{CC}(k)$ in Figure 2b. It can be observed in these figures that there is close correspondence between $\hat{\Omega}_{AA}(k)$ obtained from the explicit atom and united atom models. By contrast, the rotational isomeric state model of Suter and Flory shows ad-

ditional structure in $\hat{\Omega}_{AA}(k)$ not seen with the continuous rotation models. In particular, the shoulder seen with the rotational isomeric state model at approximately $k \approx 1$ Å^{-1} contributes to features in the low angle peak of the structure factor (discussed later) that are not seen experimentally.

Likewise, there is reasonable consistency between the united and explicit atom $\hat{\Omega}_{CC}(k)$ functions seen in Figure 2b. Not surprisingly, the discrete nature of the five-state rotational isomeric model introduces additional features in the intramolecular structure of i-PP that are not seen in the united and explicit atom models.

IV. Experimental Techniques

Wide-angle X-ray scattering experiments[17] were performed at $T = 180$ °C on i-PP samples obtained from Goodfellows Co. and on s-PP samples at $T = 183$ °C obtained from Fina Corp. The i-PP samples had a viscosity average molecular weight of $M_v = 2.80 \times 10^5$ and a total site density of 0.03282 Å^{-3}. The samples were contained in a Be cryostat filled with an inert gas to prevent oxidation. The measurements were taken in a reflection geometry with MoKα radiation ($\lambda = 0.7107$ Å) with a Zr filter placed in the incident beam and with electronic discrimination at the solid state detector. Measurements were taken in the wavevector regime $0.3 \le k \le 16$ Å^{-1}. The variation in temperature over the volume of the sample was approximately ±1−2 °C.

The experimental scattering intensities were corrected for Compton scattering, absorption, polarization, detector discrimination, and multiple scattering and were normalized to the scattering from uncorrelated, independent scattering sites to give an experimental structure factor $\hat{S}_{exp}(k)$. The self scattering contribution $\hat{S}_s(k)$

$$\hat{S}_s(k) = \sum_m b_m^2(k) \tag{8}$$

is then subtracted from the experimental structure factor. In eq 8 the $b_m(k)$ are wavevector dependent site scattering factors for the m = A, B, or C sites. Following Narten,[32] these site scattering factors can be estimated according to the expression

$$b_m(k) = \sum_{i=1}^{4} a_{mi} \exp(-B_{mi}k^2/16\pi^2) + c_m \tag{9}$$

where the constants a_{mi}, B_{mi}, and c_{mi} are taken from ref 32. The data is then reported as a normalized structure function $\hat{H}_{exp}(k)$ on a per site basis.

$$\hat{H}_{exp}(k) = \frac{\hat{S}_{exp}(k) - S_s(k)}{[b_A(k) + b_B(k) + b_C(k)]^2} \tag{10a}$$

These scattering results are shown in Figures 4−7.

V. Comparison between Theory and Experiment

For simplicity, in the computation of the single-chain structure from Monte Carlo calculations, we assumed that the bond lengths and bond angles were held fixed. In reality, these distances are not fixed but instead undergo high frequency vibrations. We can approximately correct our intramolecular structure functions to account for thermal broadening by applying a Debye−Waller correction factor[32] to the Monte Carlo results.

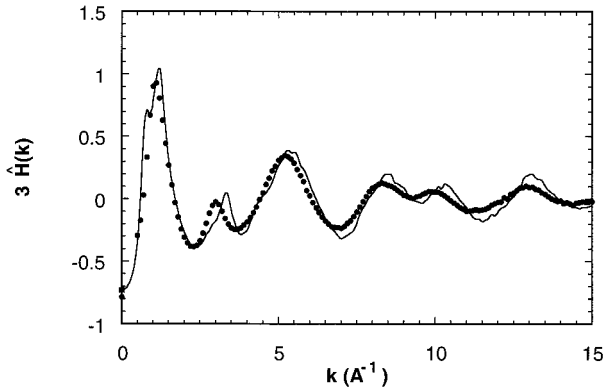

Figure 4. Comparison of theoretical and experimental structure factors defined in eqs 8−10. Points are experimental data for i-PP at 180 °C. The solid curve is from PRISM calculations using the rotational isomeric state model as input.

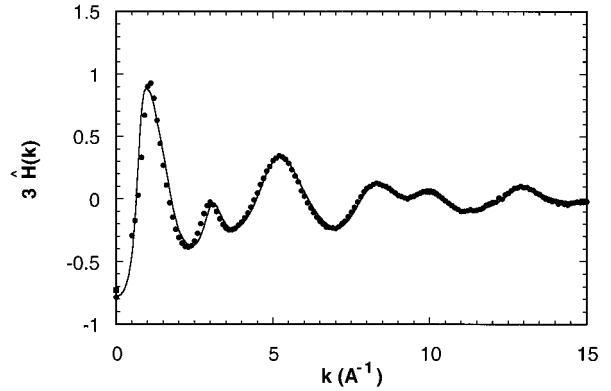

Figure 5. Comparison of theoretical and experimental structure factors defined in eqs 8−10. Points are experimental data for i-PP at 180 °C. The solid curve is from PRISM calculations using the united atom model as input.

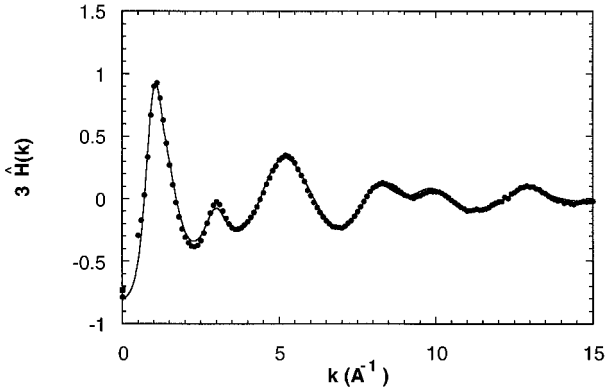

Figure 6. Comparison of theoretical and experimental structure factors defined in eqs 8−10. Points are experimental data for i-PP at 180 °C. The solid curve is from PRISM calculations using the explicit atom model as input.

This is accomplished by multiplying each of the $\omega_{ij}(k)$ terms in eq 4 by the factor $\exp(l_{ij}^2k^2/2)$ where l_{ij} is the Debye−Waller factor corresponding to a given type of vibration. In this work we set $l_{12} = 0.078$ corresponding to C−C stretching vibrations, and $l_{13} = 0.108$ corresponding to C−C−C bending based on analysis of the experimental data at high wavevector. All the remaining Debye−Waller factors were assumed to be the same and were set to $l_{14} = 0.08$ (0.14) for the united atom (explicit atom) models to get the best agreement between the intramolecular structure factor and experiment at high wavevectors. It should be emphasized that these thermal broadening corrections only affect the structure factor at large wavevector and have virtually

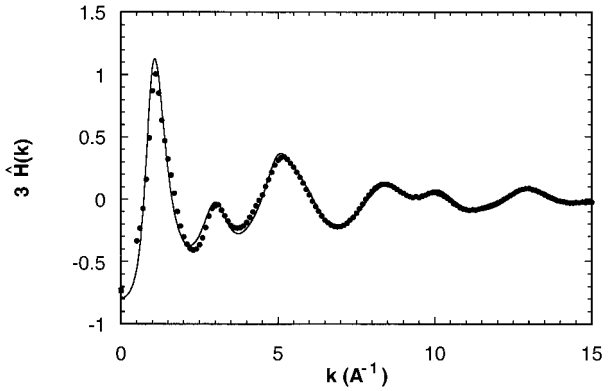

Figure 7. Comparison of theoretical and experimental structure factors defined in eqs 8−10. Points are experimental data for s-PP at 180 °C. The solid curve is from PRISM calculations using the united atom model as input.

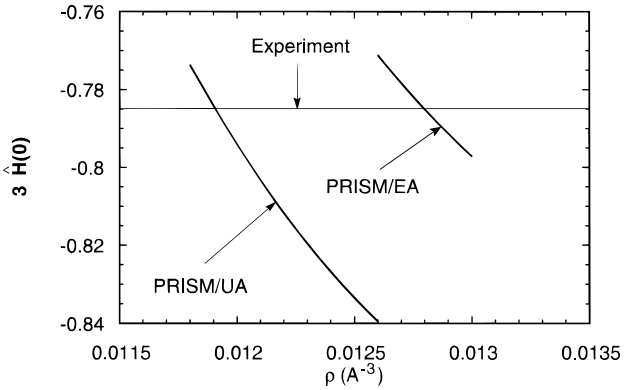

Figure 8. The zero wavevector structure factor for i-PP at 180 °C as a function of density calculated from PRISM theory with the united atom (UA) and explicit atom (EA) models. The intersection with the experimental line provides an estimate of the effective monomer density required to reproduce the experimental packing fraction.

no effect on the low wavevector behavior controlled by intermolecular packing.

In our Monte Carlo calculation of the intramolecular structure of a single chain, we have set all the nonbonded interactions between sites separated by more than five bonds to zero in order to reproduce the correct scaling of the radius of gyration with molecular weight in the melt. Obviously this cannot be rigorously correct since, even in a melt, a real chain cannot overlap with itself. A consequence of this approximation is that, due to unphysical overlaps of intramolecular sites, the packing fraction η of polymer used in the PRISM calculation is artificially lowered relative to the experimental system. We can correct[18] for this deficiency in an approximate fashion by increasing the density ρ above the experimental value of ρ_{exp} in order to recover the experimental packing fraction.

In this investigation we determined the corrected ρ in an approximate fashion by adjusting the density to recover the experimental value of the zero wavevector structure factor $\hat{H}(0)$ from PRISM theory. In Figure 8 we have plotted the PRISM predictions for $\hat{H}(0)$ as a function of monomer density. From this figure we have tabulated the density ρ needed to reproduce the zero wavevector structure factor for both the united and explicit atom models in Table 3. These densities were then subsequently used in PRISM theory to compute the complete structure factors as a function of k. An upper bound ρ^* to the corrected density can be estimated by calculating the volume of overlapping sites assuming pairwise overlaps only. This calculation is outlined in the Appendix and the results are shown in Table 3. Indeed it can be seen that our estimate of ρ from the zero wavevector structure factor falls in the expected range $\rho_{exp} \leq \rho \leq \rho^*$.

Table 3. Overlap Corrections

Model	ρ_{exp} (Å^{-3})[a]	ρ^* (Å^{-3})	ρ (Å^{-3})	Δ_o	Δ
i-PP united atom	0.01094	0.0126	0.0119	0.4752	0.0740
i-PP explicit atom	0.01094	0.0130	0.0128	0.4844	0.1235
s-PP united atom	0.01094	0.0132	0.01305	0.4912	0.0870

[a] Experimental density at 453 K estimated from the data of Zoller.[36]

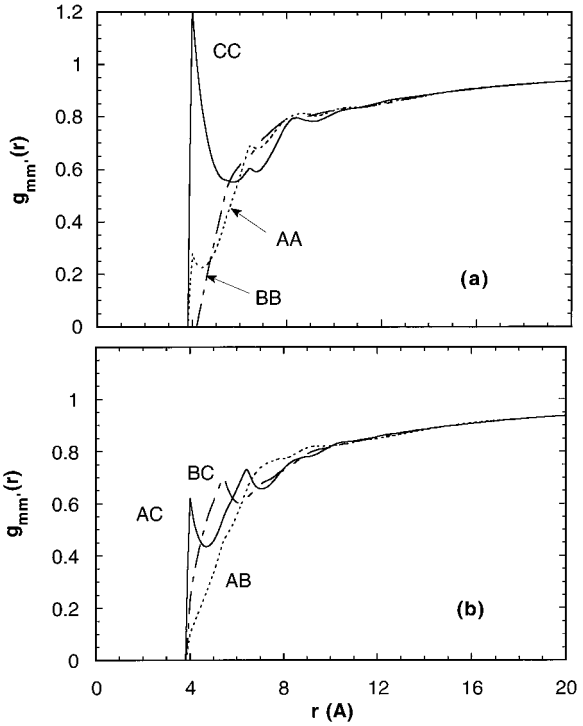

Figure 9. Intermolecular radial distribution functions computed for i-PP using the united atom model intramolecular structure functions as input. Key: (a) correlations between site of the same type; (b) correlations between unlike pairs of sites.

Six independent partial structure factors $\hat{S}_{mm'}(k)$ can be computed from PRISM theory according to the definitions

$$\hat{S}_{mm'}(k) = \rho_m \hat{\Omega}_{mm'}(k) + \rho_m \rho_{m'} h_{mm'}(k) \qquad (11)$$

In eq 11 the intramolecular functions $\hat{\Omega}_{mm'}(k)$ are provided by the single chain Monte Carlo simulations, and the intermolecular contribution $\hat{h}_{mm'}(k)$ comes directly from PRISM theory by solution of eqs 3−5. To make contact with experimental scattering we can now compute a total scattering function

$$\rho \hat{S}(k) = \sum_{mm'} b_m(k) b_{m'}(k)\, \hat{S}_{mm'}(k) \qquad (12)$$

Comparison between theory and experiment is now made for the structural function $\hat{H}(k)$ computed analogously to eq 10a.

$$\hat{H}(k) = \frac{\hat{S}(k) - S_s(k)}{[b_A(k) + b_B(k) + b_C(k)]^2} \qquad (10b)$$

Comparisons between theory and experiment are seen in Figures 4−7.

From Figure 4 it can be seen that PRISM theory for i-PP, using intramolecular functions obtained from the

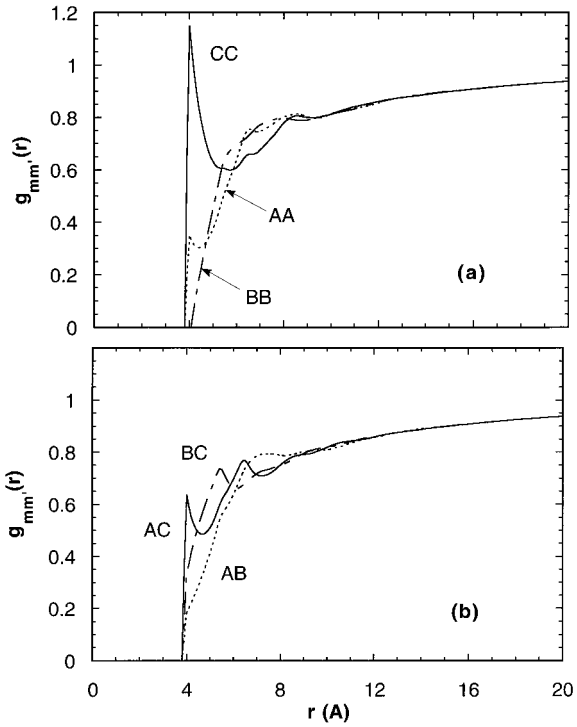

Figure 10. Intermolecular radial distribution functions computed for i-PP using the explicit atom model intramolecular structure functions as input. Key: (a) correlations between site of the same type; (b) correlations between unlike pairs of sites.

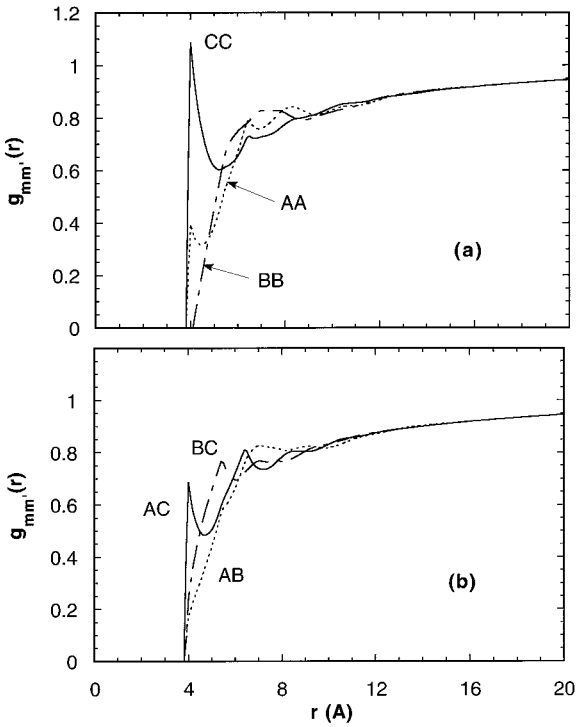

Figure 11. Intermolecular radial distribution functions computed for s-PP using the united atom model intramolecular structure functions as input. Key: (a) correlations between site of the same type; (b) correlations between unlike pairs of sites.

rotational isomeric state model of Suter and Flory, shows significant differences from the experimental points. The lowest angle peak at $k \approx 8$ Å^{-1} is particularly relevant since it contains significant contributions from the intermolecular packing. From Figure 4 it can be observed that the theory predicts two overlapping peaks in this region, whereas the experimental scattering shows only one peak. The differences at higher wavevectors ($k \geq 8$ Å^{-1}) are due in part to incorrect choices for the backbone bond angles in the Suter and Flory model[19] in Table 1. Our experience has shown that the qualitatively incorrect structure of the low angle peak persists and appears to be an inherent result when the Suter−Flory rotational isomeric state model for i-PP is used as input to PRISM theory.

In Figures 5 and 6, it can be seen that there is a much closer correspondence between theory and experiment for the united atom and explicit atom models than for the rotational isomeric state model at all wavevectors. Note, in particular, that the main scattering peak at $k \approx 1$ Å^{-1} is seen to be a single, asymmetric peak with no evidence of the composite structure obtained when the rotational isomeric state model is used as input to PRISM theory. The agreement between theory and experiment at high wavevector also suggests that the correct bond angles were used in the single-chain united and explicit atom simulations. Thus it can be seen that excellent agreement is found between experiment and the united and explicit atom PRISM theory in momentum or k-space. Note in Figure 7 that similar agreement between theory and experiment is seen for s-PP.

Now that we have a good representation of the intramolecular structure functions $\hat{\Omega}_{mm'}(k)$, we can use PRISM theory to compute the details of the intermolecular packing. The six intermolecular radial distribution functions calculated for i-PP are shown in Figures 9 and 10 for the united and explicit atom models respectively. Similarly, the radial distribution functions calculated for a united atom model of s-PP are shown in Figure 11. It is difficult, if not impossible to extract the individual site $g_{mm'}(r)$'s directly from experiment. It is possible, however, to compare theory and experiment in real space in a limited sense by defining an average intermolecular radial distribution function $g_{av}(r)$, which can be estimated from experimental scattering measurements, provided we employ the theoretical intramolecular structure functions. From eqs 8−11 we can write the expression

$$\hat{H}_{exp}(k) = \frac{\sum_{mm'} b_m(k) b_{m'}(k) [\hat{\Omega}_{mm'}(k) + \rho \hat{h}_{mm'}(k) - \delta_{mm'}]}{[b_A(k) + b_B(k) + b_C(k)]^2} \tag{13}$$

We now define an average intermolecular packing function $\hat{h}_{av}(k)$ in k-space according to

$$\rho \hat{h}_{av}(k) = \frac{\sum_{mm'} b_m(k) b_{m'}(k) \hat{h}_{mm'}(k)}{[b_A(k) + b_B(k) + b_C(k)]^2} \tag{14}$$

From eq 14 we can solve for $\hat{h}_{av}(k)$ to give

$$\rho \hat{h}_{av}(k) = \hat{H}_{exp}(k) - \frac{\sum_{mm'} b_m(k) b_{m'}(k) [\hat{\Omega}_{mm'}(k) + \delta_{mm'}]}{[b_A(k) + b_B(k) + b_C(k)]^2} \tag{15}$$

To extract the average intermolecular structure from experiment, we use the united atom results for the intramolecular structure functions $\hat{\Omega}_{mm'}(k)$ and the experimental scattering data $\hat{H}_{exp}(k)$ in eq 15. The inverse Fourier transform of $\hat{h}_{av}(k)$ then yields a measure of the intermolecular packing $g_{av}(r)$ in real space.

$$g_{av}(r) = 1 + h_{av}(r) \tag{16}$$

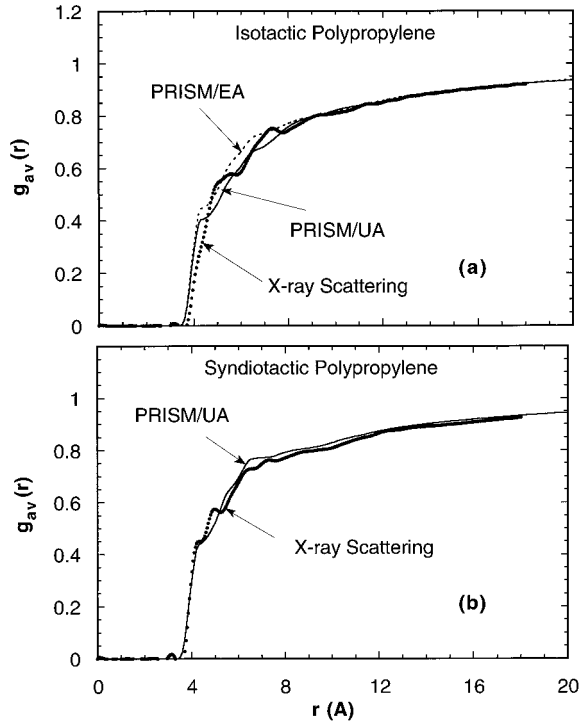

Figure 12. Comparisons between the average radial distribution function extracted from experiment with theory. Points: extracted from experiment using eqs 15 and 16: solid curve, PRISM calculations using the united atom model as input; dashed curve, PRISM calculations using the explicit atom model as input. Key: (a) i-PP; (b) s-PP.

The average intermolecular packing $g_{av}(r)$ can also be estimated from PRISM theory. For simplicity we approximate the relative wavevector dependence of the site scattering functions $b_m(k)$ as being the same for all three sites. $g_{av}(r)$ can then be calculated from PRISM theory from the individual correlations $h_{mm'}(r)$ according to

$$g_{av}(r) = 1 + \frac{\sum_{mm'} b_m b_{m'} h_{mm'}(r)}{[b_A + b_B + b_C]^2} \qquad (17)$$

where the $b_m(k)$ functions are evaluated at their zero wavevector values. A comparison of the experimental and theoretical $g_{av}(r)$ functions for both stereoregular forms of polypropylene are depicted in Figure 12. A more exact calculation, in which the explicit wavevector dependence of each site is included, yielded virtually identical results to eq 17.

VI. Discussion

A comparison between intramolecular structure functions for i-PP in Figures 2 and 3 reveals that the united and explicit atom models give very similar results. We can observe from Figure 3 in *r*-space that $\hat{\Omega}_{AA}(r)$ and $\hat{\Omega}_{CC}(r)$ show fairly sharp peaks at short distances due to pairs of sites closely spaced along the chain backbone. An analysis of the i-PP structure reveals a range of distorted trans−/trans+ configurations for adjacent rotational angles. These distorted trans dyads contribute to peaks in the AA structure (see Figure 3a) at approximately 5.0 Å and in the CC structure (see Figure 3b) at approximately 3.2 A. We also observe loosely defined trans/gauche types of configurations which contribute to peaks at approximately 4.5 Å in both the AA and CC intramolecular structure functions. The broad features at larger distances are due to pairs of sites progressively further removed from each other along the i-PP chain backbone.

An examination of Figures 5−7, comparing the various PRISM predictions for i-PP and s-PP with experimental data in *k*-space, demonstrates that both the united atom and explicit atom models agree closely with experimental X-ray scattering results. By contrast, in Figure 4 we observe that the rotational isomeric state model for i-PP of Suter and Flory, when used as input to PRISM theory, shows additional structure in the main low-angle peak that is not seen experimentally. These comparisons suggest that an accurate description of polypropylene melts requires a model with continuously varying dihedral angles. Although the explicit atom model description in Figure 6 appears to give somewhat better agreement with experiment than the corresponding united atom model in Figure 5, it is not clear that this is inherent in the model or a result of small differences in the intramolecular force fields.

The details of the intermolecular packing are captured in the six intermolecular radial distribution functions plotted in Figures 9−11. It can be seen that both the united and explicit atom models give very similar results for the packing of i-PP in the melt. It is instructive to examine these site−site correlation functions over a range of length scales. On long length scales, comparable to the radius of gyration (31.3 Å), it can be seen that all 6 of the $g_{mm'}(r)$ functions are identical. This is characteristic of the universal correlation hole regime in which intermolecular sites on two different chains are screened by other sites on those same two chains. As expected, in the correlation hole regime the packing is independent of the local details of the monomeric structure. On short length scales (<8 Å), however, we see marked differences among the site−site correlation functions which depend sensitively on the local monomeric size and shape.

On local length scales we can observe from Figures 9−11 that $g_{CC}(r)$ is very large near the distance of closest approach. This is to be expected since the pendant methyl groups are on the outside of the chain and, therefore, can approach each other unimpeded in the melt. By contrast, $g_{BB}(r)$ is zero near contact. Such behavior is due to the shielding effect the methyl group has on the backbone sites, particularly the CH moiety. In fact, examination all of the six $g_{mm'}(r)$ functions near contact are understandable qualitatively from these kinds of shielding considerations. It is expected that these nonuniversal, short-range packing details will play an important role in determining the thermodynamic and phase behavior of polypropylene melts and blends because the dispersive attractions are also short range. Thus, subtle monomeric architectural details can influence the miscibility of polymer blends through the short-range $g_{mm'}(r)$ functions.

It is interesting to compare the intermolecular packing predicted from united atom models of the two stereoregular forms of polypropylene via PRISM theory. By comparison of Figures 9 and 11, it can be seen that the packing of i-PP and s-PP in the melt is very similar. Slightly more screening is predicted in s-PP due to the pendant methyl groups leading to somewhat weaker correlations at short distances.

In Figure 12 we compare PRISM theory with the average intermolecular site−site correlation function $g_{av}(r)$ estimated from experiment via eq 17. It can be seen in Figure 12a that both the united and explicit atom models give good agreement with the experimental estimate in i-PP. Note that in contrast to the individual

site−site correlation functions, $g_{av}(r)$ is a monotonically increasing function of r without a lot of structure. Similar agreement between theory and experiment is seen in Figure 12b for s-PP.

An important limitation of the methodology used in this work arises because the Flory ideality idea is taken literally in evaluation of the intramolecular structure functions. Since repulsive interactions between intramolecular sites separated by six or more bonds are set to zero, some unphysical overlapping of remote sites occurs. As a consequence, many of the conformations allowed in the simulations occupied less volume than the actual polymer would. As discussed earlier, we correct for this unphysical overlap by using a higher monomer density in the PRISM calculations. This problem can be avoided completely by carrying out the intramolecular simulation self-consistently[18] with the PRISM intermolecular calculations.

Another limitation of invoking the Flory ideality hypothesis is that the resulting short-range van der Waals parameters needed to reproduce the correct characteristic ratio also are somewhat screened. In other words the Lennard−Jones parameters are modified in the melt in a way that also reflects the cutoff distance (six bonds) above which the excluded volume interactions are set to zero. As a result the Lennard−Jones parameters are temperature dependent and are not necessarily transferable from one molecule to another. This can be seen in Table 2 where significantly different Lennard−Jones parameters were needed for the two stereoregular forms of polypropylene. We anticipate that this difficulty will likewise be overcome to a large extent by determining the ω functions self-consistently.

In the self-consistent method one imposes a medium-induced attractive interaction, superimposed on the repulsive potential, between all pairs of sites on a single chain. This medium induced potential is calculated from PRISM theory and depends on the intermolecular packing. A single chain simulation is then performed to calculate the intramolecular structure functions $\hat{\Omega}_{mm'}(k)$. These functions are then used as input to PRISM theory to calculate a new medium-induced potential. The procedure is then repeated until a self-consistent, medium-induced potential is obtained. A modified approach is to adjust the medium-induced attractive potential until the experimental characteristic ratio of the polymer in the melt is achieved. Self-consistent calculations of this type will be the focus of future investigations.

Finally we note from Figures 9 and 11 that the intermolecular packing in the two stereoregular forms of polypropylene is very similar. It is interesting to speculate on whether the subtle differences between the intermolecular $g(r)$ functions are sufficient to drive phase separation in a blend of i-PP and s-PP. Recent diffusion measurements by Maier and co-workers[37] suggest an incompatibility between the stereoregular forms of polypropylene. PRISM theory could now be employed to predict the phase diagram for this mixture of stereoisomers in a manner similar to calculations done earlier on polyethylene/i-PP blends by Rajasekaran and co-workers.[8] This will be a topic for future investigations.

VII. Conclusions

In this investigation we performed atomistically realistic PRISM calculations on stereoregular polypropylene in the melt state. The intramolecular structure functions, required as input to PRISM theory, were determined through single-chain, Monte Carlo simulations. Excellent agreement was found between theory and wide-angle X-ray scattering experiments on isotactic polypropylene. A close correspondence was found between united atom and explicit atom models with continuously varying rotational angles. This suggests that the united atom model contains sufficiently detailed information regarding the monomeric size and shape for the purposes of PRISM calculations. The intramolecular structure functions obtained in the present investigation are thus expected to provide an accurate description of the intramolecular structure of polypropylene suitable for future PRISM calculations on polypropylene melts and blends.

Acknowledgment. The authors would like to thank J. D. McCoy and K. S. Schweizer for extremely helpful comments and suggestions.

Appendix

In this section we obtain an estimate of the upper bound ρ^* of the corrected density to compensate for unphysical overlap of sites. The packing fraction is defined to be that fraction of the total volume V that is occupied by polymer. This can be written in the form

$$\eta = \rho_{exp}(\bar{v}_A + \bar{v}_B + \bar{v}_C)(1 - \Delta_o) \tag{A1}$$

where $\bar{v}_m$ is the volume of a spherical site of type m ($=\pi d_m^3/6$). Δ_o is the intrinsic overlap fraction in the real polymer caused by our construction of the macromolecule from overlapping spherical sites.

$$\Delta_o = 1 - \frac{\bar{V}_p}{N(\bar{v}_A + \bar{v}_B + \bar{v}_C)} \tag{A2}$$

where $\bar{V}_p$ is the volume of a single macromolecule without any unphysical overlaps. Because of unphysical overlapping of sites in our Monte Carlo calculation, the packing fraction is smaller than the true packing fraction and given by

$$\eta = \rho(\bar{v}_A + \bar{v}_B + \bar{v}_C)(1 - \Delta_o - \Delta) \tag{A3}$$

where the unphysical overlaps are accounted for by the additional term Δ. The distinction between intrinsic and unphysical overlap is not exact. Since a gauche rotational state will create overlap between sites separated by three bonds, we have designated any overlap between sites connected by three bonds or less as intrinsic overlap, Δ_o. Inclusion of sites separated by four and five bonds, whose overlap is limited by Lennard−Jones potentials, results in a change in Δ_o of less than .5%.

The simplest way to calculate Δ_o and Δ is to assume that all overlap involves only two sites. The overlap fraction can then be determined through a summation over the intramolecular pair distribution function

$$\Delta,\Delta_o \le \frac{1}{V}\sum_{ij} V_{ij}(r)\omega_{ij}(r)\, d\vec{r} \tag{A4}$$

with $V_{ij}(r)$ being the overlap volume of two spherical sites i and j separated by a distance r between centers. This calculation is approximate because some of the overlap volume will be occupied by three or more sites and, therefore, will be counted more than once. This problem is particularly evident in a repeat unit, where

22% of the actual volume is occupied by three or four sites. To account for these multiple overlaps in a repeat unit correctly, a Monte Carlo integration procedure was used. A full repeat unit plus an additional A site were placed in a box. Random coordinates were generated within the three-dimensional box and the number of "hits", i.e., coordinates falling within any of the sites, was recorded. After 2×10^7 Monte Carlo steps, the volume of a repeat unit was determined by subtracting the volume of the additional A site from the integrated volume. This calculation was then combined with the overlap between pairs separated by 3 bonds to give a fairly accurate value of Δ_o. Since Δ is determined entirely by pairwise overlap, this estimate will be an upper bound to the true value.

With values for Δ_o and Δ, the packing fractions in eqs A1 and A3 can be equated to obtain

$$\rho^* \leq \rho_{exp}\left[1 - \frac{\Delta}{(1 - \Delta_o)}\right]^{-1} \qquad \text{(A5)}$$

for an upper bound to the corrected density ρ. The overlap fractions and maximum corrected densities found through the united atom and explicit atom Monte Carlo simulations are indicated in Table 3.

From the above considerations, the corrected density can be easily estimated to be in the range $\rho_{exp} \leq \rho \leq \rho^*$. An improvement upon this estimate, however, would involve considering three and higher site overlaps.

References and Notes

(1) Krishnamoorti, R.; Graessley, W. W.; Balsara, N. P.; Lohse, D. J. *Macromolecules* **1994**, *27*, 3073.
(2) Graessley, W. W.; Krishnamoorti, R.; Balsara, N. P.; Fetters, L. J.; Lohse, D. J.; Schulz, D. N.; Sissano, J. A. *Macromolecules* **1994**, *27*, 2574.
(3) Rhee, J.; Crist, B. *J. Chem. Phys.* **1993**, *91*, 4174.
(4) Bates, F. S.; Schulz, M. F.; Rosedale, J. H.; Almdal, K. *Macromolecules* **1992**, *25*, 5546.
(5) Singh, C.; Schweizer, K. S.; Yethiraj, *J. Chem. Phys.* **1995**, *102*, 2187.
(6) Singh, C.; Schweizer, K. S. *J. Chem. Phys.* **1995**, *103*, 5814.
(7) Schweizer, K. S.; Singh, C. *Macromolecules* **1995**, *28*, 2063.
(8) Rajasekaran, J. J.; Curro, J. G.; Honeycutt, J. D. *Macromolecules* **1995**, *28*, 6843.
(9) Rajasekaran, J. J.; Curro, J. G. *J. Chem. Soc., Faraday Trans.* **1995**, *91*, 2427.
(10) Honnell, K. G.; McCoy, J. D.; Curro, J. G.; Schweizer, K. S.; Narten, A. H.; and Habenschuss, A. *J. Chem. Phys.* **1991**, *94*, 4659.
(11) Narten, A. H.; Habenschuss, A.; Honnell, K. G.; McCoy, J. D.; Curro, J. G.; Schweizer, K. S. *J. Chem. Soc., Faraday Trans.* **1992,** *88*, 1791.
(12) Ballard, D. G. H.; Cheshire, P.; Longmann, G. W.; Schelten, J. *Polymer* **1978**, *19*, 379.
(13) Liesser, G.; Fischer, E. W.; Ibel, K. *J. Polym. Sci., Polym. Lett.* **1975**, *13*, 39.
(14) Weimann, P. A.; Jones, T. D.; Hillmyer, M. A.; Bates, F. S.; Londono, J. D.; Melnichenko, Y.; Wignall, G. D. Preprint.
(15) Zirkel, A.; Urban, V.; Richter, D.; Fetters, L. J.; Huang, J. S.; Kampmann, R.; Hadjichristidis, N. *Macromolecules* **1992**, *25*, 6148.
(16) Inagaki, H.; Miyamoto, T.; Ohta, S. *J. Phys. Chem.* **1966**, *70*, 3420.
(17) Londono, J. D.; Habenschuss, A.; Curro, J. G.; Rajasekaran, J. J. *J. Polym Sci.—Polym. Phys.*, in press.
(18) For recent reviews, see: Schweizer, K. S.; Curro, J. G. *Adv. Polym. Sci.* **1994**, *116*, 321. Schweizer, K. S.; Curro, J. G. *Adv. Chem. Phys.* **1997**, *98*, 1.
(19) Suter, U. W.; Flory, P. J. *Macromolecules* **1975**, *8*, 765.
(20) Schweizer, K. S.; Curro J. G. *Phys. Rev. Lett.* **1987**, *58*, 246.
(21) Curro, J. G.; Schweizer, K. S. *Macromolecules* **1987**, *20*, 1928.
(22) Curro, J. G.; Schweizer, K. S. *J. Chem. Phys.* **1987**, *87*, 1842.
(23) Chandler, D.; Andersen, H. C. *J. Chem. Phys.* **1972**, *57*, 1930.
(24) Chandler, D. in *Studies in Statistical Mechanics VIII* Montroll, E. W., Lebowitz, J. L., Eds.; North-Holland: Amsterdam, 1982.
(25) Curro, J. G. *Macromolecules* **1994**, *27*, 4665.
(26) Flory, P. J. *J. Chem. Phys.* **1949**, *17*, 203.
(27) Ballard, D. G.; Schelton, J.; Wignall, G. D.; *Eur. Polym. J.* **1973**, *9*, 965. Cotton, J. P.; Decker, D.; Benoit, H.; Farnoux, B.; Higgins, J.; Jannick, G.; Ober, R.; Picot, C.; des Cloizeaux, J. *Macromolecules* **1974**, *7*, 863.
(28) Curro, J. G. *J. Chem. Phys.* **1974**, *61*, 1203. Curro, J. G. *Macromolecules* **1979**, *12*, 463.
(29) Flory, P. J. *Statistical Mechanics of Chain Molecules*; Wiley: New York, 1969.
(30) McCoy, J. D.; Honnell, K. G.; Curro, J. G.; Schweizer, K. S.; Honeycutt, J. D. *Macromolecules* **1992**, *25*, 4905.
(31) Jorgensen, W. L.; Madura, J. D.; Swenson, C. J. *J. Am. Chem. Soc.* **1984**, *106*, 6638.
(32) Narten, A. *J. Chem. Phys.* **1979**, *70*, 299.
(33) McCoy, J. D.; Mateas, S.; Zorlu, M.; Curro, J. G. *J. Chem. Phys.* **1995**, *102*, 8635.
(34) Hwang, M.-J.; Stockfisch, T. P.; Hagler, A. T. *J. Amer. Chem. Soc.* **1994**, *116*, 2515.
(35) Honeycutt, J. D. Manuscript in preparation.
(36) Zoller, P. *J. Appl. Polym. Sci.* **1979**, *23*, 1057.
(37) Maier, R.; Thomann, R.; Kressler, J.; Mulhaupt, R.; Rudolf, B. *J. Polym. Sci. B., Polym Phys.* **1997**, *35*, 1135.

MA970500L